Tikrit Journal of Pure Science Vol. 31 (4) 2026

DOI:https://doi.org/10.25130/tjps.v31i4.2033

IRAQI Academic Scientific Journals

Tikrit Journal of Pure Science

ISSN: 1813 – 1662 (Print) --- E-ISSN: 2415 – 1726 (Online)

Journal Homepage: https://tjpsj.org/

Tikrit Journal of Pure Science

Synthesis, Properties, and Gas Sensing Performance of Chromium doped Tungsten Oxide

Wisam Hammoodi Shihab, **Abdullah M. Ali**

Department of Physics, College of Education for Pure Sciences, University of Tikrit, Tikrit, Iraq

Received: 12 May. 2025 **Received in revised forum:** 27 Jun. 2025 **Accepted:** 2 Jul. 2025

Final Proofreading: 18 Jul. 2025 **Available online:** 25 Aug. 2026

ABSTRACT

Chromium (Cr)- doped tungsten oxide (WO3) nanostructures were successfully prepared by pulse laser ablation in liquid. In order to examine the morphological, structural, and optical characteristics of Cr-doped WO_3 nanostructures and to suggest potential growth pathways, the impact of Cr content was examined. Fourier transform infrared spectroscopy (FTIR), field emission scanning electron microscopy (FESEM), and X-ray diffraction (XRD). XRD peaks confirmed the cubic structure and the reduction in crystallite size as dopant concentration increased. Surface characterization demonstrated the incorporation of chromium ions into the WO3 host lattice. The FESEM images clearly show that as doping increases, the WO3 nanoparticle size decreases. The absorption spectra show that the optical band gap energy decreases after doping and exhibit two absorption edges as the Cr concentration increases. The results showed that the sensitivity of the pure WO_3 gas sensor to (60 ppm) NO_2 at temperatures as high as (150 °C) was around (51.25 %). At around (100 °C), the maximum sensitivity of the WO3-doped (9 %) Cr gas sensor to (60 ppm) NO_2 was (24.45 %), whereas at (25 °C), the same gas sensor's maximum sensitivity was (15.64 %).

Keywords: Chromium, Gas sensor, Pulse laser ablation in liquid, Tungsten oxide.

Name: **Wisam Hammoodi Shihab** **E-mail:** wh230066pep@st.tu.edu.iq

Tikrit Journal of Pure Science Vol. 31 (4) 2026
DOI:https://doi.org/10.25130/tjps.v31i4.2033

IRAQI Academic Scientific Journals

تخليق أوكسيد التنكستن المطعم بالكروم ودراسة خصائصه التركيبية كمستشعر لغاز ثاني أوكسيد النيتروجين

وسام حمودي شهاب، عبد الله محمود علي

قسم الفيزياء، كلية التربية للعلوم الصرفة، جامعة تكريت، تكريت، العراق

الملخص

تم تحضير هياكل نانوية من أكسيد التنغستن المضاف إليه الكروم بنجاح عن طريق الاستئصال بالليزر النبضي في تقنية السائل. من أجل دراسة الخصائص المورفولوجية والبنيوية والبصرية لهياكل نانوية من أكسيد التنغستن المضاف إليه الكروم واقتراح مسارات نمو محتملة، تم فحص تأثير محتوى الكروم. أكدت مطيافية الأشعة تحت الحمراء بتحويل فورييه(FTIR) ، ومجهر مسح إلكتروني بانبعاث المجال (FESEM)، وحيود الأشعة السينية (XRD) الترتيب المكعب وانخفاض حجم البلورة مع زيادة تركيز المادة المضاف إليها. أظهرت خصائص السطح تشويب أيونات الكروم داخل الشبكات المضيفة لـ WO_3. تُظهر صور المجهر الإلكتروني الماسح بوضوح أنه عند زيادة التشويب، يتناقص حجم جسيمات WO_3 النانوية. تُظهر أطياف الامتصاص أن طاقة فجوة النطاق الضوئية تتناقص بعد التشويب وتظهر حافتي امتصاص مع زيادة تركيز الكروم. أظهرت النتائج أن حساسية مستشعر غاز WO_3 النقي لتركيز (60 ppm) من ثاني أكسيد النيتروجين عند درجات حرارة تصل إلى (150 °C) كانت حوالي (51.25 %). عند حوالي (100 °C)، بلغت أقصى حساسية لمستشعر غاز WO_3 المضاف إليه (9 %) كروم لتركيز (60 ppm) من ثاني أكسيد النيتروجين (24.45 %)، بينما عند (25 °C)، بلغت أقصى حساسية لنفس المستشعر (15.64 %).

INTRODUCTION

Nanotechnology has undergone significant advancements in recent decades, offering a new tool for innovation and progress across various fields [1]. The distinguishing characteristic is its tiny size, that reaches the nanometer scale. The materials encompass zinc, copper, gold, silver, titanium, as well as certain types of polymers and oxides such as silver oxide, cobalt oxide, titanium oxide, zinc oxide, nano carbon, graphene, silicon oxide, and more [2]. These nanomaterials have been applied in various domains, including medicine [3], industry, electronics, and environment [4]. There are two ways to prepare nanomaterials, the chemical method and the physical method, each of them includes several methods: Chemical methods include thermal decomposition, sol-gel treatment for stability [5], chemical precipitation [6] chemical vapor deposition (CVD) [7], self-assembly, chemical bath deposition (CBD), hydrothermal method (8). Physical methods include physical vapor deposition (PVD)[9], pulsed laser deposition (PLD)[10], organic metal vapor phase epitaxy (OMVPE)[11], and pulsed laser ablation in liquids (PLAL)[12]. Physical methods encompass vapor condensation[13], thermal evaporation[14]. In the same context, a nanocomposite (CS-TiO_2-Ag) was prepared via PLAL and its properties, as well as its medical and environmental applications were studied. Laser beam provides the capacity to accurately transfer large energy amounts to confined areas of a material in order to achieve the required response [15]. The material there absorption of the laser beam to have an effect on it. This absorption is remarkable in the process of laser-material interaction. This absorption process is a major source of energy within the material, this main source, shows that the beam of laser released from the source determines what occurs to the

IRAQI Academic Scientific Journals

laser-irradiated material [16]. Aim of study is to prepare and characterize the gas sensor device morphological characteristics and optical. The pulse laser ablation (PLA) technology was used to produce the gas sensor. Chromium doped tungsten oxide was prepared as sensors for nitrogen dioxide pollution gases.

MATERIALS AND METHODS

Target materials included tungsten oxide (WO_3) powder with a greater purity of (99.9 %) and chromium (Cr) powder (99.99 %) from Sigma-Aldrich. A glass beaker filled with (10 mL) of deionized water was used to make nano WO_3 and nano Cr solutions. First, 500 radiation shots were applied to pure WO_3 and Cr plates, producing nano WO_3 and nano Cr solutions. After that, laser ablation was used on the WO_3 plate while it was submerged in (5 mL) of deionized water. The WO_3 plate was subsequently replaced with the Cr plate in the same amount of deionized water. The PLA process uses a target material in a beaker and a Q-switched Nd: YAG laser (China manufacture). The angle at which the (720 mJ) concentrated laser beam strikes the item, which is (90°). Q-switched Nd: YAG laser with a wavelength of (1064 nm) (pulse width: 10 ns), a repetition frequency of (10 Hz) working under deposition conditions, and (10 cm) separated the target and the laser source. Using the drop casting process, these produced solutions were used to form thin films on a porous silicon (syntheses at 10 mA direct electric current and 10 minutes from n-type silicon) substrate as a gas sensor sample. This was accomplished by thoroughly cleaning a (1 by 1 cm^2) of silicon substrate to get rid of any dirt or spots.

The sensors' ability to sense gases was tested using a homemade gas-sensing system. There were electrical feeds through the base plate. The heating on the base plate was adjusted to bring the tested sample up to the required operating temperatures. The current passing through the heating element was monitored using a relay with programmable ON/OFF time intervals. The internal gas concentration of the system was achieved by injecting a known volume of test gas using a gas flow meter. A digital millimeter was used to measure the current passing over the sensors after they were exposed to a constant voltage. Air was allowed to enter the chamber after every gas exposure cycle. field emission scanning electron microscopy (FESEM) inspect F50 SEM business was used to analyze the morphology of the samples. The average crystallite size and crystal structure were measured using XRD (X-ray diffraction) 6000 SHIMADZ manufactured in Japan.

RESULTS AND DISCUSSION

The different amounts of Cr doped WO_3 in the deposited films are investigated using the weight difference method. Drop casting solutions derived from pulse laser-ablated nanoparticles were used to prepare the thin films. The samples were prepared by dropping the solution on pours silicon substrates and annealed at (200 °C) for two hours. The crystalline character of the deposited films has been determined using XRD examination. Figure (1) shows the XRD patterns of the pure and Cr-doped WO_3 thin films that were generated with varying Cr concentrations. The results showed that the sample had a polycrystalline structure, which could be the reason for each peak observed. The diffraction peaks are caused by the WO_3 planes of (001), (200), (112), (202), (211) and (032), and they matched the observed values of JCPDC 85-2460[17, 18], confirming the cubic phase of the deposited thin layers. But in Cr-doped WO_3 films, a new peak with a plane of (110) appears at about (44.2°), and its intensity increases with increasing Cr concentration[17]. The full width at half maximum (FWHM), inter-planar distance (d_{hkl}), and crystalline size (C.S.) are displayed in Table (1). FWHM (β) of the best orientation diffraction peak can be used to calculate the crystalline size using the Scherrer equation[19]. The findings suggest that, in some circumstances, it is possible to create nanocrystalline material. Better crystallization of the materials is implied by smaller crystalline sizes and higher FWHM values.

DOI:https://doi.org/10.25130/tjps.v31i4.2033

Additionally, because the doping process raised the tensile stress, it was discovered that the average crystal size rose somewhat as the concentration of Cr increased. Tensile stress in thin films can result from changes in bond length, local symmetries, and micro-inhomogeneities in the deposited material.

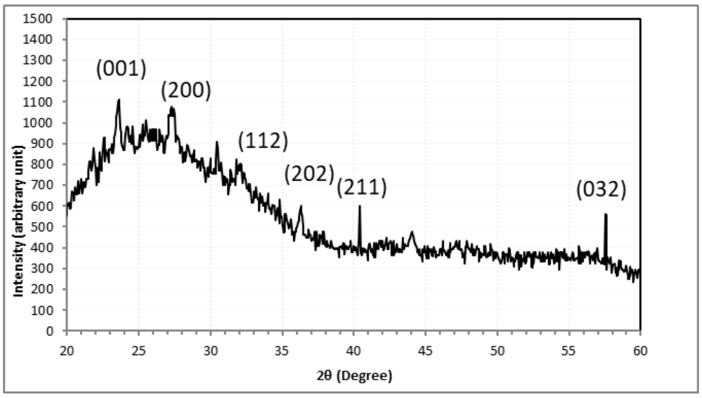

Fig. 1: XRD patterns of Cr doped WO_3 thin films prepared by pulse laser ablation in liquid.

Table 1: Structural parameters: Inter-planar spacing, crystalline size of Cr doped WO_3 thin films prepared by pulse laser ablation in liquid.

2θ (Deg.)	β (Deg.)	C.S (nm)	d_{hkl} (Å)	Phase	hkl
23.48	0.45	18.0	3.7858	Cubic	001
27.34	0.45	18.2	3.2594	Cubic	200
32.04	0.3	27.6	2.7912	Cubic	112
36.39	0.18	46.5	2.4669	Cubic	202
40.13	0.1	84.6	2.2452	Cubic	211
44.2	0.35	24.5	2.0474	Cubic	110

Figure (2) shows thin films of tungsten oxide (WO_3) doped with (3, 6, and 9 %) chromium. The FESEM image shows nanostructures similar to sponge cavities, which are more evident when the Cr doping is (3 %). The nanostructures are aligned and evenly distributed. This results in the appearance of extended surfaces, some of which are aligned with the nanoparticle and scattered along the substrate, as seen in the image of the (9 %) doped sample. The surface is covered in tiny granular particles, as shown in the FESEM image, yet there are no visible fractures. Nevertheless, occasionally white areas showed up on the film's surface. Analyses employing XRD and FESEM reveal that the particles are incredibly tiny, spherical, and around (55.19 nm) for (3 %) Cr doped WO_3, (51.07 nm) for (6 %) Cr doped WO_3, and (41.46 nm) for (9 %) Cr doped WO_3.

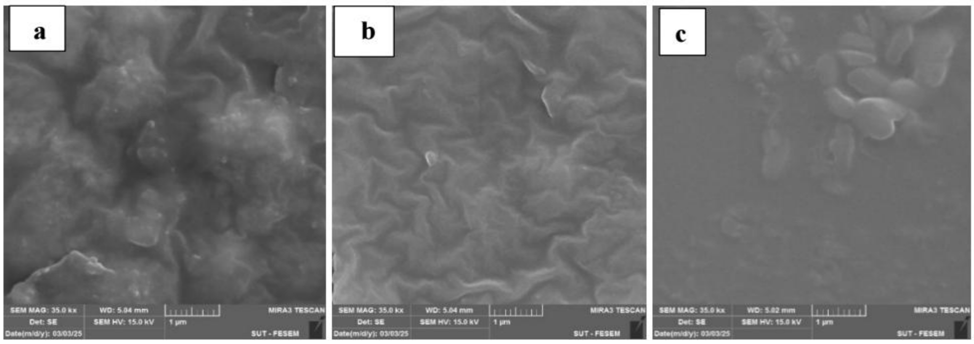

Fig. 2: FESEM image of Cr doped WO_3 thin films at different doping concentration: (a) 3%, (b) 6%, (c) 9%.

DOI:https://doi.org/10.25130/tjps.v31i4.2033

Fourier transform infrared spectroscopy (FTIR) spectroscopy was used to examine the chemical bonding arrangement of tungsten oxide nanostructures. The samples' FTIR spectra are displayed in Figure (3). These spectra show a wide absorption band in the (400–4000 cm^{-1}) wavenumber region, which is ascribed to the W–O bond vibration modes and confirms the tungsten oxide production. The presence of this distinctive band in the FTIR spectra of every sample suggests that their chemical structures are rather comparable. These band's component peaks' bonding assignments revealed that the W–O antisymmetric stretching vibration is associated with the strong adsorption peak at (827 cm^{-1}), the W–O–W low peak stretching vibration at (657 cm^{-1}), and the W–O bending vibration at (603 and 599 cm^{-1}) [20]. The as-prepared sample's FTIR spectrum also reveals a significant adsorption peak at (505 cm^{-1}), which is related to the antisymmetric stretching vibration of Cr(III)-O, and another at (835 cm^{-1}), which is related to the bending vibration of Cr(III)-O-H [21]. Bending vibrations in unbound water molecules are responsible for the peak at (1635 cm^{-1}). The H-O-H stretching vibration is represented by the band that spans (1700 to 2100 cm^{-1}). The chemical adsorption of water dissociation is the source of the other peaks, which are located at (2800 to 3500 cm^{-1}) and are caused by OH stretching on the water surface [22].

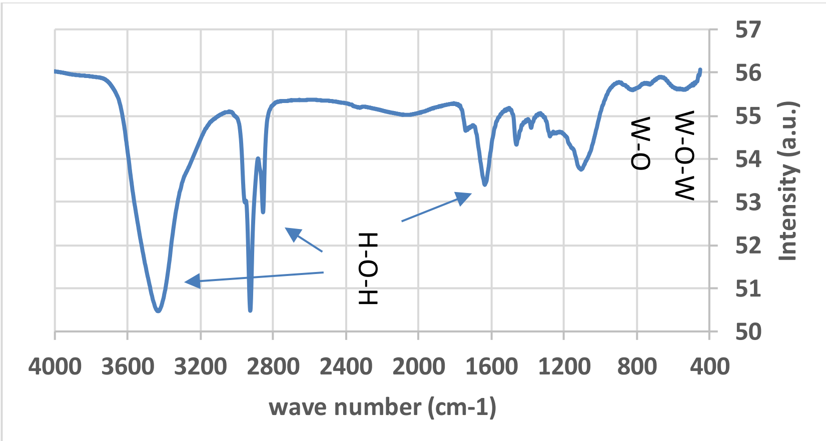

Fig. 3: FTIR spectra of syntheses Cr (6 %) doped WO_3.

Various weight percentages of Cr-doped WO_3 nanostructure (NS) were recorded for the UV-visible spectrophotometer. Figure (4) shows the overlay absorption spectra of pure WO_3 (3%, 6%, and 9 %) and Cr-doped WO_3 nanostructures. The greatest absorptivity of the pure WO_3 nanostructure was measured at (330 nm) represents as energy gap (Eg1) [23]. Furthermore, the chromium-doped tungsten oxide shows higher absorption than the pure sample, with two absorption edges displaying two different energy gaps (Eg1 and Eg2) as shown in Table (2). The first energy gap (Eg1) shows the greatest effect of tungsten oxide compared to chromium, as it causes the energy band to shift towards longer wavelengths with increasing chromium concentration. The second energy gap (Eg2) shows a greater effect of chromium when Cr is added to WO_3 nanostructures, it captures O_2 − and O− ions by forming Cr_2O_3 on the nano matrix, which helps move electrons to the WO_3 surface. The increasing absorbance of the nanoparticles from (330 nm) to the visible range (800 nm) is what causes this redshift in the spectrum[24].

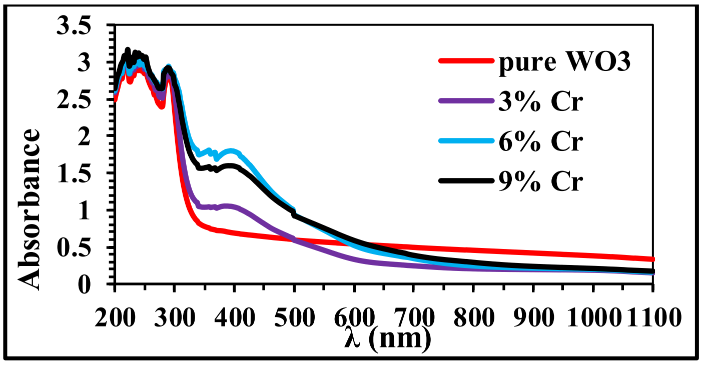

Fig. 4: UV-Vis absorbance spectra of syntheses Cr doped WO_3 at different doping concentration.

Table 2: UV-Vis parameters of syntheses Cr doped WO_3 at different doping concentration.

Sample	T%	α (cm^{-1})	K	n	ε_r	ε_i	Eg1 (eV)	Eg2 (eV)
pure	35.68	20612	0.135	2.587	6.673	0.696	3.75	---
3 % Cr	62.89	9276	0.061	2.401	5.762	0.291	3.65	1.88
6 % Cr	58.37	10769	0.070	2.492	6.205	0.350	3.26	1.82
9 % Cr	52.83	12763	0.083	2.579	6.644	0.430	3.10	1.77

Figure (5) displays the visible photoluminescence (PL) spectra region of Cr (6 %) doped WO_3 samples. (320 nm) was the excitation wavelength. Two peaks in the sample are centered at wavelengths of (470 and 700 nm), respectively, with energy gaps of (2.63 and 1.77 eV). This outcome is in line with the findings we found in the UV-Vis spectrum, which shows two absorption peaks: one in the visible spectrum's blue region and the other its red region. Due to the fact that PL is an emission spectrum and UV-Vis is an absorption spectrum, the optical energy gap values in the two tests differ.

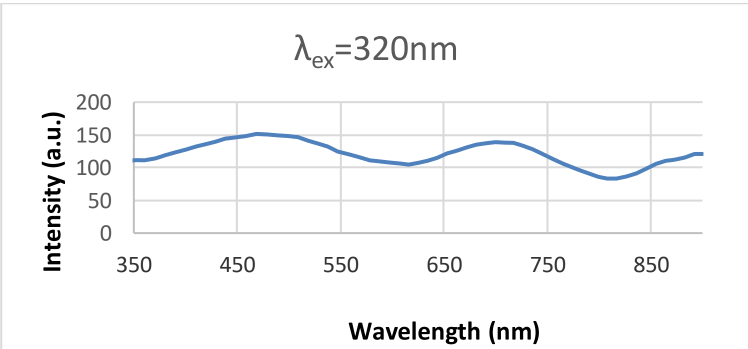

Fig. 5: PL spectra of Cr (6%) doped WO_3 samples.

The obtained pure WO_3 and doped Cr gas sensors coated on glass substrates are shown to have sensitivity to NO_2 gas as a function of temperature in Figure (6). Utilizing an oxidizing gas, such as NO_2, at a concentration of (60 ppm) at working temperatures of (25, 100, and 150 °C). As seen in Figure (1), the pure WO_3 sensor is more sensitive to (60 ppm) of NO_2. The air-mixed ratio was around (51.25 %) at temperatures up to (150 °C) [25, 26]. When exposed to (60 ppm) NO_2, the produced WO_3 doped (9 %) Cr gas sensor's maximum sensitivity may reach (24.45 %) at around (100 °C), whereas at (25 °C), it can achieve (15.64 %) [17]. All of the aforementioned findings demonstrate that gas sensors' sensitivity to the oxidizing gas has significantly increased. The increasing quantity of surface adsorbed oxygen species and the nano-sized WO_3 particle on the glass substrate are the causes [25].

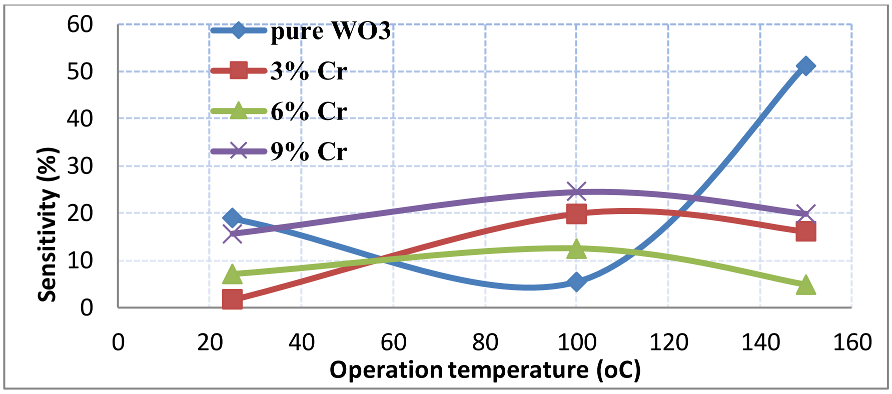

Fig. 6: The variation of sensitivity with the operating temperature of the prepared pure WO_3 and doped Cr to NO_2 gas.

The resistance changes of pure WO_3 exposed to (60 ppm) NO_2 over time is depicted in Figure (7). When exposed to NO_2 gas suddenly, the resistance drops to a constant condition. Pure WO_3 exhibits selective behavior toward NO_2 gas, whereas doped and n-type WO_3 are converted to p-type based on the PLAL synthesis procedure [26, 27]. The adsorption of NO_2 gas on the surface may have achieved a saturation point, as shown by the rapid change in electrical resistance over time for Cr doped WO_3 to reach a saturation state in Figure (7) when the gas is on. The samples' resistance decreased when NO_2 gas was applied to their surface. The sample shows selective behavior for different gases as a result of this behavior.

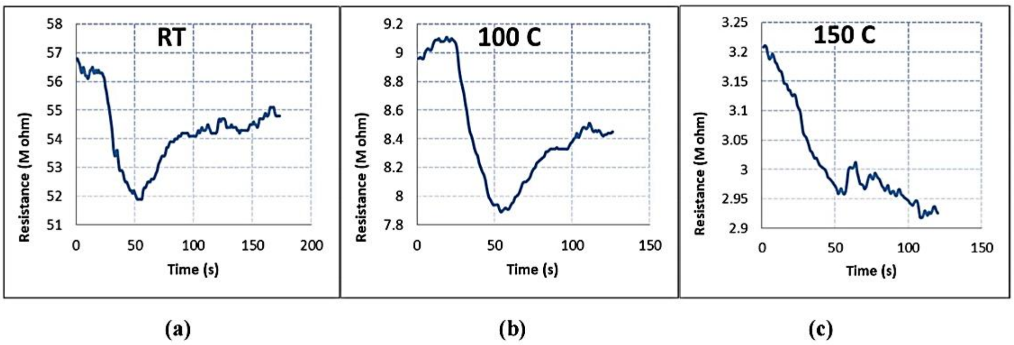

Fig. 7: The variation resistance with time for different operation temperature of NO_2 gas for the WO_3 doped Cr (6 %) (a) RT, (b) 100C, and (c) 150C.

CONCLUSIONS

This work demonstrates a clear example of how to prepare clean and chromium-doped tungsten oxide thin films using pulse laser ablation in liquid. PLAL is the best method for producing Cr doped WO_3 since its cost-effective produces no byproducts, and emits no odors. It may be concluded that the substantial reduction in the energy gap was due to the action of the doping material, and that this alteration renders the material an extremely efficient medium for application in UV photodetectors and gas sensors. The FESEM results demonstrated the presence of average-sized nanoparticles and the presence of a nanostructure on the surface. They demonstrated NO_2 gas with enhanced sensitivity, quicker reaction, and a slower sensor recovery time.

Conflict of interest: The authors of this work declare that they have no conflicts of interest.

Sources of funding: This work was supported by ongoing institutional funding. No additional grants to carry out or direct this particular research were obtained

Author contribution: Each co-author has made unique contributions to the work. The author WHS prepared the thin films and contributed to writing the article, and wrote the program for gas sensor properties. As the author AMA, he supervised the work, contributed to the analysis of the results. and reviewed the article draft.

REFERENCES

1. KK W, PV C, WL A. Introduction to Nanomaterials. Carbon Nanostructures2024. p. 1-15.
2. Abdul-Jabbar N, M.Ibrahim I, Fezaa H. The effect of gold Nanoparticles on Structural and Electrical properties of WO3 thin films. Tikrit Journal of Pure Science. 2023;23(2):114-22. http://dx.doi.org/10.25130/tjps.23.2018.036
3. Hashim AF, Ibrahim FT, Razeg KH. SiO2@ Cu core: antibacterial," shell" active agents synthesized through sol-gel. Global Journal of Engineering and Technology Advances. 2023;14(02):141-9. https://doi.org/10.30574/gjeta.2023.14.2.0034
4. Haunsbhavi K, Kumar KDA, Mele P, Aldossary OM, Ubaidullah M, Mahesh H, et al. Pseudo n-type behaviour of nickel oxide thin film at room temperature towards ammonia sensing. Ceramics International. 2021;47(10):13693-703. https://doi.org/10.1016/j.ceramint.2021.01.230
5. Al Khudhair A, Bouchmella K, Andrei RD, Mehdi A, Mutin PH, Hulea V. One-step non-hydrolytic sol-gel synthesis of mesoporous SiO2-Al2O3-NiO catalysts for ethylene oligomerization. Microporous and Mesoporous Materials. 2021;322:111165. https://doi.org/10.1016/j.micromeso.2021.111165
6. Mhamdi H, Azaiez K, Fiorido T, Zaghouani RB, Lazzari J, Bendahan M, et al. Room temperature NO2 gas sensor based on stain-etched porous silicon: Towards a low-cost gas sensor integrated on silicon. Inorganic Chemistry Communications. 2022;139:109325. https://doi.org/10.1016/j.inoche.2022.109325
7. Hassan RA, Ibrahim FT. Preparation and characterization of anatase titanium dioxide nanostructures as smart and self-cleaned surfaces. Iraqi Journal Of Applied Physics. 2020;16(4). https://doi.org/10.1007/s11468-020-01205-8
8. Hashim AE, Ibrahim FT. A Novel Design for Gas Sensor of Zinc Oxide Nanostructure Prepared by Hydrothermal Annealing Technique. Chemical Methodologies. 2023;7(4):314-24. https://doi.org/10.22034/chemm.2023.377977.1634
9. Helmersson U, Lattemann M, Bohlmark J, Ehiasarian AP, Gudmundsson JT. Ionized physical vapor deposition (IPVD): A review of technology and applications. Thin solid films. 2006;513(1-2):1-24. https://doi.org/10.1016/j.tsf.2006.03.033
10. Ahmed B, Mohammad S, Mohammed G. The Effect of Laser Energy on the Structural, Optical and Electrical Properties of CdO Nanomaterials Generated Using (PLD) Technology, and Fabrication a Gas Sensor. Tikrit Journal of Pure Science. 2024;29:107-18. http://dx.doi.org/10.25130/tjps.v29i1.1451
11. Özgür Ü, Alivov YI, Liu C, Teke A, Reshchikov MA, Doğan S, et al. A comprehensive review of ZnO materials and devices. Journal of applied physics. 2005;98(4). https://doi.org/10.1063/1.1992666
12. Kadhim RG, Ali AK, Noori MF. Nanofabrication and characterization of gold metal by pulsed laser ablation in SDS solution. Advances in Physics Theories and Applications. 2012;11:23-7.
13. DM M. The Foundations of Vacuum Coating Technology [Internet]2003.
14. El E, Odeh M, Mahmoud A. Influence of Thickness on Structural and optical properties of the CdS single crystal nano structure thin films Deposited Via Thermal evapovation. Tikrit Journal of Pure Science. 2019;24:98. http://dx.doi.org/10.25130/tjps.v24i6.443
15. Milan M, Laserna J. Diagnostics of silicon plasmas produced by visible nanosecond laser ablation. Spectrochimica Acta Part B: Atomic Spectroscopy. 2001;56(3):275-88. https://doi.org/10.1016/S0584-8547(01)00158-6
16. Beena D, Lethy K, Vinodkumar R, Pillai VM, Ganesan V, Phase D, et al. Effect of substrate temperature on structural, optical and electrical properties of pulsed laser ablated nanostructured

indium oxide films. Applied Surface Science. 2009;255(20):8334-42. https://doi.org/10.1016/j.apsusc.2009.05.057

17. Chang X, Dong X, Liu X, Tong Y, Li K, Li Z, et al. Constructing a hexagonal/orthorhombic WO3 phase junction for enhanced photochromism. Optical Materials. 2023;142:114131. https://doi.org/10.1016/j.optmat.2023.114131

18. Zhang H, Wang J, Liu X, Ma X, Zhu W. Hydrothermal synthesis of pure-phase hierarchical porous hexagonal WO3 microspheres as highly efficient support for Pd catalyst for hydrogenation. Particuology. 2018;41:126-32. https://doi.org/10.1016/j.partic.2018.01.014

19. Rusu D, Rusu G, Luca D. Structural characteristics and optical properties of thermally oxidized zinc films. Acta physica polonica A. 2011;119(6):850-6.

20. Tehrani FS, Ahmadian H, Aliannezhadi M. Hydrothermal synthesis and characterization of WO3 nanostructures: Effect of reaction time. Materials Research Express. 2020;7(1):015911. https://doi.org/10.1088/2053-1591/ab66fc

21. Yang J, Martens WN, Frost RL. Transition of chromium oxyhydroxide nanomaterials to chromium oxide: a hot-stage Raman spectroscopic study. Journal of Raman Spectroscopy. 2011;42(5):1142-6. https://doi.org/10.1002/jrs.2773

22. Ratnasamy P, Leonard A. Structural evolution of chromia. The Journal of Physical Chemistry. 1972;76(13):1838-43. https://doi.org/10.1021/j100657a009

23. Adimule V, Bowmik D, Adarsha H. A facile synthesis of Cr doped WO3 nanocomposites and its effect in enhanced current-voltage and impedance characteristics of thin films. Letters on Materials. 2020;10(4):481-5.

24. Jerold Antony A, Mary Jelastin Kala S, Joel C, Biju Bennie R, Vivetha S. Structural, optical, and magnetic properties of pristine and Cr doped WO3 nanoparticles. Inorganic and Nano-Metal Chemistry. 2022;52(7):951-60. https://doi.org/10.1080/24701556.2021.2025395

25. Shendage S, Patil V, Vanalakar S, Patil S, Harale N, Bhosale J, et al. Sensitive and selective NO2 gas sensor based on WO3 nanoplates. Sensors and Actuators B: Chemical. 2017;240:426-33. https://doi.org/10.1016/j.snb.2016.08.177

26. Aamir L. Novel p-type Ag-WO3 nano-composite for low-cost electronics, photocatalysis, and sensing: synthesis, characterization, and application. Journal of Alloys and Compounds. 2021;864:158108. https://doi.org/10.1016/j.jallcom.2020.158108

27. Yao G, Yu J, Wu H, Li Z, Zou W, Zhu H, et al. P-type Sb doping hierarchical WO3 microspheres for superior close to room temperature ammonia sensor. Sensors and Actuators B: Chemical. 2022;359:131365. https://doi.org/10.1016/j.snb.2022.131365